VIA MEDICA

ORIGINAL ARTICLE

Folia Morphol.
Vol. 84, No. 1, pp. 83–96
DOI: 10.5603/fm.99585

ISSN 0015–5659
eISSN 1644–3284
journals.viamedica.pl

Morphometric evaluation of the left atrioventricular valve complex and its clinical relations

Buse Naz Çandır[1, 2], Çağla Ergin[3], Kader Yılar[1], Osman Coşkun[1], Erdoğan Kara[3], Ayşin Kale[1], Nilgün Bozbuğa[4], Adnan Öztürk[1, 5], Özcan Gayretli[1]

[1]*Department of Anatomy, Istanbul Faculty of Medicine, Istanbul University, Istanbul, Türkiye*
[2]*Department of Anatomy, Faculty of Medicine, Istanbul Yeni Yuzyil University, Istanbul, Türkiye*
[3]*Morgue Department, Council of Forensic Medicine, Istanbul, Türkiye*
[4]*Department of Cardiovascular Surgery, Istanbul Faculty of Medicine, Istanbul University, Istanbul, Türkiye*
[5]*Department of Anatomy, Istanbul Health & Technology University, Istanbul, Türkiye*

[Received: 28 February 2024; Accepted: 28 May 2024; Early publication date: 3 June 2024]

Background: *This study aims to evaluate morphometrically and morphologically the left fibrous ring, mitral leaflets, tendinous cords, and papillary muscles, which are the components of the left atrioventricular valve complex (LAVC), and to reveal their clinical relationships.*

Materials and methods: *A total of 120 human hearts were examined at the Forensic Medicine Institute. The study included cases aged 30 years and older, less than 24 hours post-mortem. Heart length, width, height/width ratio, anteroposterior and mediolateral diameters of the annulus, annular area, length and width of leaflets, number and attachment sites of tendinous cords, number, shape, length, the width of papillary muscles, and distances to various points were recorded to determine their spatial configurations. Additionally, the measurement data of LAVC components in cases with and without cardiovascular disease (CVD) and their relationships with the demographic characteristics of the cases were also explained.*

Results: *In the diagnostic performance test (ROC analysis), it was determined that body mass index (> 26.7), heart weight (> 414 g), heart height/width ratio (≤ 1.24), mitral valve width (> 99.96 mm), left ventricular wall thickness (> 15.08 mm), annular area (> 619.37 mm^2), and mediolateral diameter of the annulus (> 30.71 mm) are important diagnostic criteria in determining CVD if they are outside the specified reference values.*

Conclusions: *This study provides anatomical information about LAVC, along with recommendations for diagnosis and surgical treatment planning. We believe that our findings will be useful to clinicians.* (Folia Morphol 2025; 84, 1: 83–96)

Keywords: left atrioventricular valve complex, left fibrous ring, mitral leaflets, tendinous cords, papillary muscles, cardiovascular disease

Address for correspondence: Buse Naz Çandır, Millet Caddesi, İstanbul Tıp Fakültesi Hastanesi, Anatomi Anabilim Dalı, 118-K, 34093, Fatih, İstanbul, Türkiye; tel. 90(554)2051001, e-mail: busenazcandir@gmail.com

INTRODUCTION

The mitral valve (MV) is one of the four main valve structures of the heart, located between the left atrium (LA) and left ventricle (LV). The left atrioventricular valve complex (LAVC), on the other hand, is a structure complex consisting of left fibrous ring (LFR), anterior mitral leaflet (AML), posterior mitral leaflet (PML), tendinous cords (TC), and superior papillary muscle (SPM) and inferior papillary muscle (IPM) of the left ventricle. The LAVC is one of the most complex mechanical structures of the human body [19]. It is not just a passive flap protecting the left atrioventricular orifice, but a set of components that work actively and in coordination throughout the cardiac cycle [5, 11, 15]. The ability of the LAVC to function effectively and accurately depends on the biomechanical and structural integrity of its components.

Mitral valve dysfunction has a variable aetiology and might result from pathological changes in any component of the LAVC [19]. Bringing the pathological mitral valve to normal functioning requires understanding the structure and dysfunction caused by the disease [5]. There are many studies in the literature investigating the structure of the LAVC, primarily through cadaver studies using formalin-fixed heart specimens or imaging methods. However, unlike previous studies, this study used unfixed fresh hearts. The aim was to examine the morphometric and morphological aspects of the LAVC components and the LV as a whole in these heart specimens, compare these characteristics in healthy and pathological cases, and uncover various characteristics that can be associated with clinical outcomes.

MATERIALS AND METHODS

The prospective study was carried out between January 2021 and November 2022 at the Forensic Medicine Institute after ethics committee approval (IRB: 2021/376). Inclusion criteria for the study were age (over 30) and absence of thoracic or cardiac trauma (penetrating, firearm etc.). Exclusion criteria included time (autopsy performed more than 24 hours postmortem), burns, foreign nationalities, and identification or history of previous cardiac surgery/ /intervention. One hundred and twenty cases met inclusion and exclusion criteria.

Cases with causes of deaths unrelated to the heart and those showing pathological findings/artefacts related to cardiopulmonary resuscitation or postmortem changes were considered as healthy. A total of 31 cases that showed pathological cardiac findings during macroscopic and histopathologic examinations were considered as "Cardiovascular Disease" (CVD). These findings included an increase in heart size, severe subepicardial fattening, and myocardial infarction (pearlescent-white discoloration, fibrosis, aneurysm, granulation, and trabecular changes).

Morphometric evaluations were made with a 0.01 mm precision digital calliper (Insize 1112-150, Insize Co. Ltd, Germany). Area and angle measurements were made using the Image J Program (http:// rsbweb.nih.gov/ij). Measurement references are explained in Table 1. All evaluations were conducted by two experienced researchers, and the two measured values were averaged. Measurements were repeated if there were more than 10% differences between the two values.

Statistical analysis

The conformity of the variables to the normal distribution was examined using the Shapiro-Wilk Test. If the variables fit the normal distribution, mean ± standard deviations were used; if they did not fit the normal distribution, median values were presented with minimum and maximum values. The Independent Samples *t*-Test or Mann–Whitney U-Test was used for comparisons between two groups according to the results of the normality test. If the number of groups was three or more, the ANOVA test or the Kruskal–Wallis test was used. Categorical variables were specified as n (%) and were compared between groups using the Pearson Chi-Square Test, Fisher's Exact Chi-Square Test, and Fisher's Freeman-Halton Test. Logistic Regression Analysis was performed to determine the factors influencing the pathological results of the cases. The established Logistic Regression Model was found to be significant ($p < 0.001$). Receiver-Operator Characteristic (ROC) Analysis was conducted to investigate the diagnostic performance of the parameters. The SPSS (IBM Corp. Released 2012; IBM SPSS Statistics for Windows, Version 21.0. Armonk, NY, USA), and MedCalc Programs were used for statistical analysis and $p < 0.05$ was considered statistically significant.

RESULTS

Among the 120 subjects included in the study, 21.67% (n = 26) were female and 78.33% (n = 94) were male. The mean age of women was 44.3 ± ± 14.4 years, and the mean age of men was 54.5 ±

Table 1. Measurement references.

	Parameters	Measurement references
Heart and left ventricle	Heart length [mm]	Vertical distance from the highest point of the left auricle of heart to the apex of heart in the sagittal plane
	Heart width [mm]	The largest horizontal distance between the right atrium and left ventricle in the coronal plane
	Heart length/width ratio	The ratio of the length of the heart to the width of the heart
	MV width [mm]	Width measurement of the MV at LFR level
	LV wall thickness [mm]	Transverse wall thickness measurement 2 cm inferior to the point where the MV attaches to the lateral wall of the left ventricle
	Apex wall thickness [mm]	Thickness measurement of the deepest point of the left ventricle (which coincides with the apex of heart from the outside)
	LVIT [mm]	Distance from the MV to the deepest point of the left ventricle (apex of heart)
	LVOT [mm]	Distance from deepest point of left ventricle (apex of heart) to AV
	LVOT 1st diameter [mm]	Distance from the septal wall of the left ventricle to the ventricular surface of the AML, at the level of the bases of the semilunar leaflets of aortic valve
	LVOT 2nd diameter [mm]	Distance from the septal wall of the left ventricle to the ventricular surface of the AML, 0.5 cm below the bases of the semilunar leaflets of aortic valve
Left fibrous ring	AP diameter of annulus [mm]	Distance measurement of the LFR in the anteroposterior direction
	ML diameter of annulus [mm]	Distance measurement of the LFR in the mediolateral direction
	Annular area [mm^2]	LFR area measurement
Mitral leaflets	Annular distance of mitral leaflets [mm]	Attachment line distances of AML, PML (P1, P2, P3) ALC and PMC to LFR
	Height of mitral leaflets [mm]	The distance from the midpoint of the annular distances of the AML, PML (P1, P2, P3), ALC, and PMC to the midpoints of their free edges
Tendinous cords	Number of TTC	Number of TTC originating from each muscle
	Origin and attachment sites of TC	Origin and insertion sites of TC
	Number of FTC	Number of FTC in left ventricle
Papillary muscles	Number of muscles	Each muscle with its own base, trunk, and one or more apex was considered a PM. Muscles belonging to the SPM and IPM groups were numbered from the LVOT to the free wall of the left ventricle.
	Number of apexes	Number of apex in each muscle
	Height of muscle [mm]	Length measurement from base to highest apex of each muscle group
	Width of muscle [mm]	Width measurement in horizontal plane of the base part, where the muscle group connects to the left ventricle
	Highest apex-LFR distance [mm]	Vertical distance of the highest apex of each muscle group to the LFR
	Distance between bases [mm]	Horizontal distance between the midpoints of the bases of the SPM-IPM muscle groups
	Distance between apexes [mm]	Horizontal distance between highest apexes of SPM-IPM muscle groups
	PM-AAM distance [mm]	The distance of the midpoints of the bases of the muscle groups to the midpoint of the anterior portion of the LFR (AAM)
	PM-coaptation distance [mm]	The distance of the midpoints of the bases of the muscle groups to the coaptation line (the line of apposition of the rough areas where the tendinous cords attach on the ventricular surfaces of the leaflets)
	Intermuscular angle º	Angle between the lines drawn from the midpoints of the bases of the SPM and IPM muscle groups to the AAM
	Shapes of muscles	Cone (one apex), bifurcated (two apex), trifurcated (three apex), truncated (more than three apex), and flat-top (with no significant height difference between apexes)
	Origin regions of muscles	The left ventricle was divided along its length into three sections: upper, middle, and lower. It was recorded from which 1/3 part each muscle originated.

AAM — anterior annular midpoint; ALC — anterolateral commissure; AML — anterior mitral leaflet; AV — aortic valve; FTC — false tendinous cords; IPM — inferior papillary muscle; LFR — left fibrous trigone; LV — left ventricle; LVIT — left ventricular inflow tract; LVOT — left ventricular outflow tract; MV — mitral valve; PML — posterior mitral leaflet; PM — papillary muscle; PMC — posteromedial commissure; SPM — superior papillary muscle; TC — tendinous cords; TTC — true tendinous cord.

Table 2. Death event of the cases.

	Pathological group (n = 31)	Non-pathological group (n = 89)
Hanging	0	13 (14.61%)
Gunshot wound	1 (3.23%)	7 (7.87%)
Cerebral haemorrhage	0	1 (1.12%)
Fall to the ground	2 (6.45%)	7 (7.87%)
Deterioration of health	8 (25.81%)	4 (4.49%)
Drug poisoning	0	1 (1.12%)
Sharp object injury	0	4 (4.49%)
Methyl alcohol intoxication	1 (3.23%)	2 (2.25%)
Be found dead	10 (32.26%)	16 (17.98%)
Postoperative	0	1 (1.12%)
Fall ill	7 (22.58%)	8 (8.99%)
Drowning in water	0	2 (2.25%)
Traffic accident	1 (3.23%)	14 (15.73%)
Falling from height	1 (3.23%)	9 (10.11%)

Data are expressed as numbers n (%).

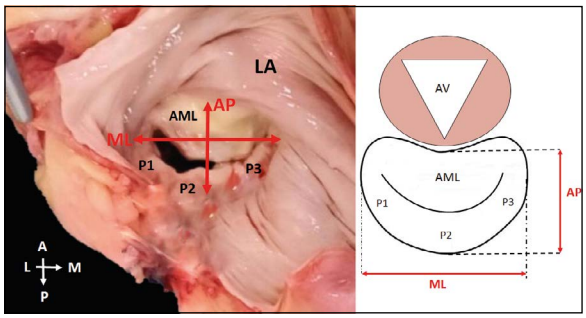

Figure 1. Left fibrous ring measurements. A — anterior; P — posterior; L — lateral; M — medial; LA — left atrium; AP — anteroposterior; ML — mediolateral; AV — aortic valve; AML — anterior mitral leaflet.

± 15.6 years (52.3 ± 15.8 years for all cases). The cases were divided into three groups based on age: 30–44 years old (n = 41, 32.5%), 45–59 years old (n = = 40, 33.3%), and 60 years and older (n = 39, 34.2%), considering cardiovascular risk factors. Additionally, according to their body mass index (BMI) values, the cases were divided into three groups: low (< 18.5, n = 6, 5%), normal (18.5–24.9, n = 41, 34.2%), and high (> 24.9, n = 73, 60.8%). Among the 31 pathological cases, 2 (6.45%) were female, 29 (93.55%) were male. Among the 89 non-pathological cases, 24 (26.97%) were female and 65 (73.03%) were male. The mean age of the pathological cases was 60.16 ± ± 13.34, and the mean age of the nonpathological group was 49.58 ± 15.78 years.

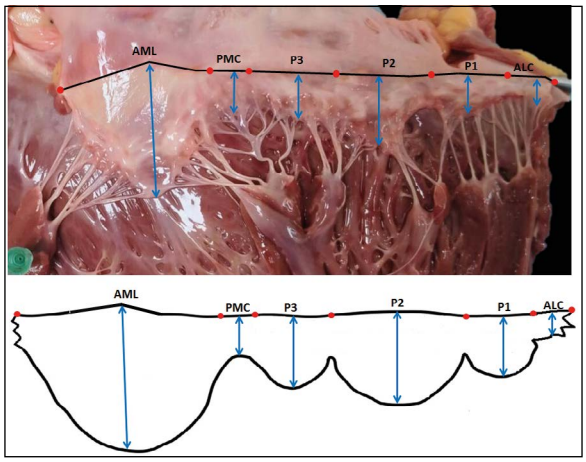

Figure 2. Mitral leaflets measurements. Blue arrows — height of leaflets, black lines between red dots — annular distance of leaflets. AML — anterior mitral leaflet; ALC — anterolateral commissure; PMC — posteromedial commissure.

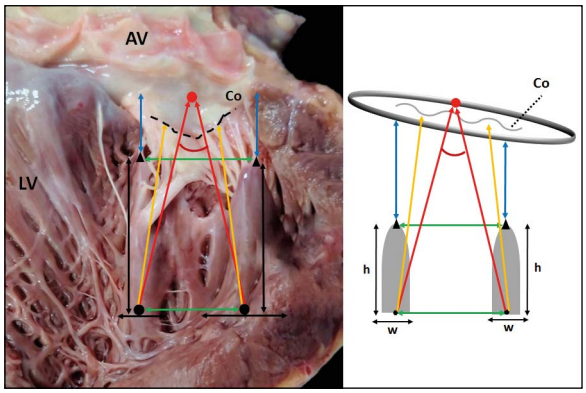

Figure 3. Papillary muscle measurements. Black vertical arrows — muscle height; black horizontal arrows — muscle width; black dots — the midpoint of the muscle bases; black triangles — highest apex points; red dots — anterior annular midpoints; green arrows — distance between bases and distance between apexes; red arrows — muscle base-anterior annular midpoint distance; red angle — intermuscular angle; yellow arrows — muscle base-coaptation line distance; blue arrows — highest apex-annulus distance. AV — aortic valve; LV — left ventricle; Co — coaptation line.

The death events of the cases are presented in Table 2. A difference was detected between the pathological conditions of the cases ($p = 0.003$). Subgroup analysis revealed that the rate of death due to hanging was higher in the non-pathological group, while the rate of deterioration of health and falling ill was higher in the pathological cases ($p < 0.05$).

The measurements of the heart and LV, LFR (Fig. 1), mitral leaflets (Fig. 2), CT, PM numbers and measurements (Fig. 3), and the comparison of these measurements with the demographic characteristics and pathological conditions of the cases are presented in Tables 3–8, respectively. Additionally, shapes and

Table 3. Heart and left ventricle measurements.

	Sex			Age				BMI				Pathological condition		
	Female (n = 26)	**Male (n = 94)**	**p value**	**< 45 (n = 41)**	**45–59 (n = 40)**	**60 and older (n = 39)**	**p value**	**Low (n = 6)**	**Normal (n = 41)**	**High (n = 73)**	**p value**	**Pathologic (n = 31)**	**Non-pathologic (n = 89)**	**p value**
Heart weight	279 (175:449)	407 (240:735)	**< 0.001**[c]	320.41 ± 76.84	426.25 ± 112.75	425.38 ± 112.43	**< 0.001**[g]	306.67 ± 93.51	340.93 ± 87.25	424.10 ± 114.18	**< 0.001**[g]	503.52 ± 98.93	350.20 ± 87.79	**< 0.001**[d]
Heart length	88.94 (75.53:107.67)	101.75 (81.45:182)	**< 0.001**[c]	98.36 (75.53:118.64)	101.13 (79.31:182)	99.17 (83.65:119.14)	0.522[f]	87.32 (81.31:117.69)	95.32 (75.53:120.80)	101.82 (79.31:182)	**0.003**[f]	107.67 (88.51:182)	96.28 (75.53:119.14)	**< 0.001**[c]
Heart width	74.16 (62.66:97.35)	85.50 (61.42:115.04)	**< 0.001**[c]	77.32 (64.91:112.58)	83.06 (62.66:115.04)	85.42 (61.42:112.40)	**0.010**[f]	82.08 ± 8.42	79.75 ± 10.19	85.97 ± 10.60	**0.010**[g]	93.77 ± 8.68	80.12 ± 8.97	**< 0.001**[d]
Heart length/ /width ratio	1.21 (1.02:1.45)	1.20 (0.99:2.24)	0.633[c]	1.24 (1.02:1.45)	1.20 (0.99:2.24)	1.14 (1.01:1.38)	**0.016**[f]	1.09 (1:1.25)	1.23 (1.02:1.45)	1.18 (0.99:2.24)	**0.020**[f]	1.14 (0.99:2.24)	1.22 (1:1.45)	**0.009**[c]
MV width	90.44 ± 13.25	100.58 ± 12.86	**0.001**[d]	92.53 ± 10.19	102.31 ± 14.81	100.50 ± 13.53	**0.002**[g]	102.92 ± 10.66	93.75 ± 13.80	100.60 ± 13.08	**0.023**[g]	105.73 ± 12.48	95.82 ± 13.03	**<0.001**[d]
LV wall thickness	11.54 ± 1.55	13.27 ± 2.05	**< 0.001**[d]	12.32 ± 1.62	13.13 ± 2.43	13.27 ± 2.03	0.084[g]	12.48 (10.63:15.97)	12.15 (8.96:16.54)	13.32 (8.22:19.55)	**0.002**[f]	34.16 ± 5.10	30.96 ± 4.26	**< 0.001**[d]
Apex wall thickness	1.93 (1.06:5.54)	2.60 (1.09:5.59)	**< 0.001**[c]	2.27 (1.16:4.96)	2.54 (1.06:5.59)	2.59 (1.09:5.54)	0.223[f]	2.71 (1.67:3.29)	2.24 (1.06:5.59)	2.68 (1.09:5.54)	**0.021**[f]	3.02 (1.75:5.12)	2.31 (1.06:5.59)	**0.002**[c]
LVIT	71.05 (54.89:92.56)	79.88 (28.39:110.70)	**< 0.001**[c]	77.78 ± 9.84	78.69 ± 9.80	75.80 ± 14.03	0.515[g]	62.58 (56.17:78.07)	75.64 (28.39:96.49)	80.05 (57.97:110.70)	**< 0.001**[f]	84.34 (63.63:110.70)	75.66 (28.39:101.50)	**< 0.001**[c]
LVOT	71.79 (55.64:83.98)	76.12 (18.91:107.70)	**0.016**[c]	75.65 (60.20:102.16)	76.62 (55.64:103.46)	71.50 (18.91:107.70)	0.128[f]	60.63 (55.08:76.23)	74 (18.91:103.46)	78.65 (54.05:107.70)	**< 0.001**[f]	82.47 (60:107.70)	74 (18.91:99.42)	**< 0.001**[c]
LVOT 1st diameter	12.07 (8.13:31.59)	14.90 (5.95:27.94)	**0.029**[c]	12.01 (8.13:31.59)	15.46 (9.33:26.15)	15.19 (5.95:27.94)	**0.001**[f]	14.23 (8.88:25.03)	12.49 (8.13:27.94)	15.42 (5.95:31.59)	0.120[f]	16.34 (10.01:26.15)	13.57 (5.95:31.59)	**< 0.001**[c]
LVOT 2nd diameter	14.33 (8.17:33.13)	17.55 (10.55:28.46)	**0.001**[c]	15.85 (8.17:33.13)	17.50 (12.19:27.50)	18.41 (10.55:28.46)	**0.004**[f]	17.13 (10.73:25.88)	16.57 (11.67:28.46)	18.38 (8.17:33.13)	0.129[f]	19.12 (13.89:27.89)	16.39 (8.17:33.13)	**< 0.001**[c]

Data are expressed as median (minimum:maximum) and mean ± standard deviation in grams for heart weight and in mm for other parameters. [c]Mann–Whitney U test, [d]the independent samples t-test; [f]Kruskal–Wallis test; [g]ANOVA test. MV — mitral valve; LV — left ventricle; LV — left ventricle; LVIT — left ventricular inflow tract; LVOT — left ventricular outflow tract; MV — mitral valve.

Table 4. Left fibrous ring measurements.

	Sex			Age				BMI				Pathological condition		
	Female (n = 26)	Male (n = 94)	p value	< 45 (n = 41)	45–59 (n = 40)	60 and older (n = 39)	p value	Low (n = 6)	Normal (n = 41)	High (n = 73)	p value	Pathologic (n = 31)	Non-pathologic (n = 89)	p value
AP diameter of annulus	19.76 ± 3.24	22.63 ± 5.09	**0.001**[d]	19.59 (13.33:34.47)	22.50 (12.35:35.84)	23.03 (11.62:33.59)	**0.003**[g]	26.25 (16.09:33.59)	20.55 (15.45:31.78)	22.08 (11.62:35.84)	0.340[f]	22.70 (11.62:35.84)	21.23 (12.35:34.47)	0.529[e]
ML diameter of annulus	30.09 ± 5.28	32.26 ± 4.43	**0.036**[d]	30.35 ± 4.22	32.73 ± 5.39	32.34 ± 4.10	**0.048**[g]	35.20 (21.54:38.36)	31.07 (21.68:43.52)	31.53 (23.67:47.44)	0.155[f]	34.16 ± 5.10	30.96 ± 4.26	**0.001**[d]
Annular area	520.12 ± 136.71	633.65 ± 162.51	**0.001**[d]	538.36 (324.79:1026.75)	644 (352.16:1060.97)	637.79 (319.66:992.18)	**0.005**[f]	736.51 (352.16:992.18)	560.53 (319.66:904.17)	619.37 (324.79:1060.97)	0.126[f]	657.84 (347.56:1060.97)	578.14 (319.66:1026.75)	**0.039**[e]

Data are expressed as median (minimum:maximum) and mean ± standard deviation in mm for diameter measurements and mm² for area measurements. [d]Mann–Whitney U test; [e]the independent samples t-test; [f]Kruskal–Wallis test; [g]ANOVA test; AP — anteroposterior; BMI — body mass index; ML — mediolateral.

origin regions of papillary muscles (PMs) are shown in Fig. 4 and 5.

Logistic regression analysis was conducted to determine the risk factors affecting the presence of disease in the cases included in the study (Tab. 9). Independent variables were included in the regression model by using the forward selection method.

The results of ROC analysis applied to determine the pathology groups showed that BMI, heart weight, heart length/width ratio, MV width, VS wall thickness, annulus mediolateral (ML) diameter, and annular area values can be used as diagnostic markers in determining the pathology groups. However, the annulus anteroposterior (AP) diameter cannot be used in this respect ($p = 0.547$) (Tab. 10).

DISCUSSION

Heart and left ventricle measurements

According to Gray's [25], the length and width of the heart were defined as 12 cm and 8.5 cm, and the mean heart weight was 280–340 g in men and 230–280 g in women, respectively. Mohammadi et al. [17] examined the heart sizes in 550 cadavers and found the mean heart length to be 11.41 ± 2.15 cm, heart width to be 8.21 ± 4.38 cm, and heart weight to be 248.96 g in men and 242.74 g in women. They stated that these values were associated with the age, height and body weight of the cadavers, but not with gender and BMI. We believe that the age difference between the sample groups explains the difference between the two studies (Tab. 3). Additionally, cases with the length/width index ≤ 1.24 were more likely to have CVD.

When studies in different races were reviewed, it was found that the MV width was 7 to 10.1 cm on average in healthy individuals [17]. In this study, the mean MV width in healthy subjects was found to be 9.5 cm (Tab. 3), and it was noted that cases with this value > 99.96 mm were more likely to be pathological.

For the heart to maintain its normal physiology, the wall thickness must be proportional to the systolic pressure and ventricular width [8, 14]. It was reported that available data on this structural anatomy are limited [27]. Our findings are consistent with previous studies [14], and it was observed that the probability of CVD was high in cases with LV wall thickness > 15.08 mm.

Left ventricular inflow tract (LVIT) and left ventricular outflow tract (LVOT) are markers reflecting

Table 5. Mitral leaflets measurements.

	Sex			Age				BMI				Pathological condition		
	Female (n = 26)	**Male (n = 94)**	**p value**	**< 45 (n = 41)**	**45–59 (n = 40)**	**60 and older (n = 39)**	**p value**	**Low (n = 6)**	**Normal (n = 41)**	**High (n = 73)**	**p value**	**Pathologic (n = 31)**	**Non-pathologic (n = 89)**	**p value**
AML annular distance	32.34 ± 4.54	35.41 ± 4.53	**0.003**[d]	33.05 ± 4.14	35.73 ± 5.27	35.51 ± 4.18	**0.016**[g]	37.27 ± 5.83	34.07 ± 5.28	34.91 ± 4.20	0.264[g]	36.16 ± 4.50	34.25 ± 4.68	0.051[d]
PMC annular distance	6.11 (3.75:12.20)	6.75 (3.72:11.90)	0.087[c]	6.23 (3.84:12.20)	7.13 (3.75:11.90)	6.50 (3.72:9.41)	0.064[f]	5.50 (3.98:8.13)	6.23 (3.72:10.60)	6.88 (3.75:12.20)	0.208[f]	7.18 (4.06:11.20)	6.36 (3.72:12.20)	**0.036**[c]
P3 annular distance	12.21 (5.97:20.60)	15.30 (7.21:30.00)	**0.031**[c]	12.32 (7.40:24.30)	15.25 (7.21:30)	16.10 (5.97:28.79)	**0.019**[f]	13.65 (9.34:23.70)	13.20 (7.25:30)	15.50 (5.97:25.70)	0.281[f]	16.60 (7.21:24.30)	13.70 (5.97:30)	**0.002**[c]
P2 annular distance	23.91 ± 6.61	25.58 ± 7.88	0.325[d]	24.17 ± 6.91	26.02 ± 8	25.49 ± 8	0.536[g]	26.86 ± 7.60	24.00 ± 7.25	25.77 ± 7.84	0.429[g]	27.46 ± 8.74	24.43 ± 7.08	0.056[d]
P1 annular distance	8.82 (4.93:19.80)	10.37 (4.77:29.35)	0.051[c]	9.19 (5.01:19.84)	10.09 (4.93:22.12)	10.59 (4.77:29.35)	0.222[f]	8.73 (8.04:29.35)	8.77 (4.77:19.80)	10.57 (4.93:22.12)	**0.020**[f]	10.96 (7.70:19.84)	9.28 (4.77:29.35)	**0.024**[c]
ALC annular distance	4.56 (3.12:9.52)	5.64 (3.17:10.88)	**0.019**[c]	5.49 (3.12:10.88)	5.85 (3.74:9.85)	5.28 (3.17:9.02)	0.109[f]	4.65 (3.74:5.47)	5.15 (3.12:9.85)	5.80 (3.33:10.88)	**0.005**[f]	5.95 (4.13:9.04)	5.47 (3.12:10.88)	0.144[c]
AML height	22.89 ± 3.01	26.27 ± 3.69	**< 0.001**[d]	24.96 ± 4.23	25.79 ± 3.47	25.88 ± 3.71	0.488[g]	24.89 ± 3.58	24.56 ± 4.08	26.14 ± 3.59	0.095[g]	27.15 ± 3.47	24.97 ± 3.78	**0.006**[d]
PMC height	7.45 (3.69:11.65)	7.91 (4.57:15.25)	**0.032**[c]	7.74 (4.56:11.62)	7.80 (4.57:15.25)	7.87 (3.69:12.61)	0.862[f]	7.20 (4.57:8.62)	8.02 (4.56:11.98)	7.74 (3.69:15.25)	0.538[f]	7.94 (6.42:12.61)	7.74 (3.69:15.25)	0.535[c]
P3 height	9.20 (5.37:13.26)	10.25 (7.08:19.39)	**0.001**[c]	9.69 (6.54:14.58)	10.06 (7.41:18.70)	10.26 (5.37:19.39)	0.237[f]	10.14 (8.53:10.61)	9.77 (6.82:15.73)	9.92 (5.37:19.39)	0.615[f]	10.18 (7.12:19.39)	9.82 (5.37:18.70)	0.370[c]
P2 height	12.35 (9.92:16.89)	13.42 (8.17:21.30)	**0.004**[c]	13.58 (9.96:18.80)	12.56 (8.17:21.30)	13.20 (9.92:19.79)	0.362[f]	12.98 (10.22:18.53)	13.21 (10.21:17.73)	13.15 (8.17:21.30)	0.934[f]	12.65 (8.17:21.30)	13.41 (9.92:21.27)	0.523[c]
P1 height	10.25 ± 2.21	11.27 ± 2.09	**0.032**[d]	10.85 (6.77:15.58)	10.51 (7.50:16.31)	11.13 (6.75:15.99)	0.654[f]	11.76 ± 1.73	11.11 ± 1.90	10.96 ± 2.32	0.667[g]	11.04 ± 2.42	11.05 ± 2.06	0.984[d]
ALC height	10.22 (6.75:15.58)	11.03 (7.50:16.31)	**0.014**[c]	6.48 (3.81:11.07)	6.46 (4.03:10.68)	6.87 (4.33:10.66)	0.288[f]	6.46 (5.07:8.44)	6.32 (3.81:11.07)	6.70 (4.03:10.68)	0.529[f]	6.87 (4.06:10.68)	6.33 (3.81:11.07)	0.062[c]

Data are expressed as median (minimum:maximum) and mean ± standard deviation in mm. [c]Mann–Whitney U Test; [d]the independent samples t-test; [f]Kruskal–Wallis test; [g]ANOVA Test. ALC — anterolateral commissure; AML — anterior mitral leaflet; BMI — body mass index; PMC — posteromedial commissure.

Table 6. Tendinous cords measurements.

Origin sites	Attachment sites	Pathological group (n = 31)				Non-pathological group (n = 89)				p value
		Mean ± SD	Median	Min	Max	Mean ± SD	Median	Min	Max	
SPM	AML	4.9 ± 2.4	4	2	14	5.3 ± 2.5	5	2	14	0.801[c]
	ALC	1.3 ± 0.5	1	1	3	1.2 ± 0.5	1	1	3	0.121[c]
	P1	3.1 ± 1.2	3	1	6	3.2 ± 1.4	3	1	10	0.913[c]
	P2	2.7 ± 1.2	2	1	5	2.4 ± 1.1	2	1	6	0.265[c]
IPM	AML	4.8 ± 1.4	5	2	7	5.0 ± 1.4	5	2	9	0.623[c]
	PMC	1 ± 0.2	1	0	1	1.1 ± 0.3	1	1	3	0.058[c]
	P3	3.1 ± 1.3	3	1	6	3.3 ± 1.5	3	1	8	0.707[c]
	P2	2.4 ± 1.5	2	1	7	2.7 ± 1.3	2	1	7	0.122[c]

Data expressed as numbers (n). [c]Mann–Whitney U test. AML — anterior mitral leaflet; ALC — anterolateral commissure; IPM — inferior papillary muscle; PMC — posteromedial commissure; SPM — superior papillary muscle.

Table 7. Papillary muscle numbers.

		Pathological group (n = 31)					Non-pathological group (n = 89)				
		SPM									
		1	2	3	4	T	1	2	3	4	T
IPM	1	12	2	0	0	14	29	7	1	1	38
	2	9	1	0	0	10	24	6	1	0	31
	3	5	0	0	1	6	10	6	0	0	16
	4	1	0	0	0	1	3	1	0	0	4
	T	27	3	0	1	31	66	20	2	1	89

Data are expressed as numbers (n). IPM — inferior papillary muscle; SPM — superior papillary muscle; T — total.

the preload and afterload of the heart. Especially the LVOT carries a risk of stenosis or obstruction due to its narrower and more complex channel or tunnel structure [23], causing a decrease in the compliance (flexibility) and diastolic function of the LV, depending on the degree of obstruction [2]. This might result in heart failure, stroke or sudden cardiac death [2, 23]. Although the LVIT and LVOT distances are well defined, there is no definite consensus on the reference point for LVOT diameter measurement, possibly because LVOT obstruction may be at the valvular or subvalvular level [26]. Therefore, diameter measurements were performed at both levels in this study. LVIT and LVOT distances and diameters were found to be related to the pathological conditions of the cases ($p < 0.001$).

Left fibrous ring

The left fibrous ring is the key structure in replacement surgeries [6], and it has been reported that maintaining an appropriate ratio between the AP and ML diameters of the LFR is extremely important for the prevention of mitral regurgitation [15]. In direct annuloplasty techniques (Cardioband, Mitraline, etc.), it is observed that the AP diameter of the annulus is focused on the placement of anchors to reduce the size of the mitral annulus [1], and anchor disengagement has been reported in a considerable number of cases [16]. In this study, it was observed that only the ML diameter of the annulus was associated with pathological groups ($p = 0.001$) and could be used as a marker in the diagnosis of CVD (Tab. 10). Therefore, clinical trials that investigate the potential of ML diameter in surgeries to reduce mitral annulus dimensions may be planned.

Annular area is 4–6 cm^2 in healthy adults [18]. While an annular area smaller than 2 cm^2 indicates mitral stenosis [18], the annular area may increase significantly in mitral regurgitation [5, 7]. In these cases, the original shape of the ring and its sphincter feature change, resulting in increased stress on the mitral leaflets [7]. As expected, the annular area was larger in pathological cases in this study. It was also found that the probability of CVD is higher in cases with an annular area value > 619.37 mm^2.

Mitral leaflets

Mitral leaflets are divided into anterior (AML), posterior (PML), and lateral sections (commissuras) according to their shape and annular connections [5, 11]. Carpentier [4] defined three mussel-like structures of the PML as P1 laterally, P2 in the middle, and P3 medially, and the corresponding regions in the AML as A1, A2, and A3. Commissural structures are

Table 8. Papillary muscles measurements.

	Sex			Age				BMI				Pathological condition		
	Female (n = 26)	Male (n = 94)	p value	< 45 (n = 41)	45–59 (n = 40)	60 and older (n = 39)	p value	Low (n = 6)	Normal (n = 41)	High (n = 73)	p value	Pathologic (n = 31)	Non-pathologic (n = 89)	p value
SPM muscle number	1 (1:3)	1 (1:4)	0.934[c]	1 (1:2)	1 (1:4)	1 (1:4)	0.481[f]	1 (1:2)	1 (1:3)	1 (1:4)	0.366[f]	1 (1:4)	1 (1:4)	0.156[c]
SPM apex number	3 (1:5)	3 (1:9)	0.736[c]	3 (1:5)	3 (1:9)	3 (1:6)	**0.010[f]**	3 (2:3)	3 (1:5)	3 (1:9)	0.692[f]	3 (1:9)	3 (1:6)	0.982[c]
SPM height	33.07 (19.46:48.56)	33.70 (3.13:68.43)	0.369[c]	33.17 (3.13:47.29)	35.56 (19.06:58.64)	32.56 (13.48:68.43)	0.310[f]	28.48 (16.12:42.91)	31.93 (3.13:42.40)	35.63 (19.46:68.43)	**0.002[f]**	38.31 (19.06:68.43)	32.97 (3.13:53.80)	**0.005[c]**
SPM width	17.34 (11.35:26.43)	18.13 (8.46:44.69)	0.566[c]	17.04 (11.02:35.16)	19 (10.49:44.69)	16.69 (8.46:39.55)	0.110[f]	19.32 (14.20:25.03)	16.25 (8.46:44.69)	18.26 (10.33:39.55)	0067[f]	18.68 (10.49:39.55)	17.45 (8.46:44.69)	0.356[c]
SPM highest apex-LFR	15.96 (7.91:26.18)	21.55 (0:31.29)	**< 0.001[c]**	19.66 (7.91:31.29)	20 (0:26.67)	22.29 (4.26:30.37)	0.079[f]	19.19 (13.10:22.44)	20.16 (7.91:30.21)	21.60 (0:31.29)	0.174[f]	21.07 (0:28.02)	20.71 (4.26:31.29)	0.771[c]
IPM muscle number	2 (1:4)	2 (1:4)	0.929[c]	2 (1:4)	2 (1:4)	1 (1:4)	0.141[f]	1.50 (1:3)	2 (1:3)	2 (1:4)	0.866[f]	2 (1:4)	2 (1:4)	0.850[c]
IPM apex number	4.50 (2:6)	4 (2:8)	0.639[c]	4 (2:7)	4 (3:6)	4 (2:8)	0.611[f]	4 (3:8)	4 (2:7)	4 (2:6)	0.554[f]	4 (2:8)	4 (2:7)	0.459[c]
IPM height	29.34 ± 5.89	33.66 ± 7.54	**0.008[d]**	32.56 (19.46:52.24)	31.64 (15.62:49.11)	33.91 (17.13:59.57)	0.754[f]	25.14 (22.87:37.24)	30.49 (17.13:45.56)	34.28 (15.62:59.57)	**0.006[f]**	37.27 ± 8.05	31.14 ± 6.51	**< 0.001[d]**
IPM width	16.53 (9.93:21.75)	19.14 (9.99:38.16)	**0.007[c]**	18.70 (11.70:36.23)	18.48 (9.93:38.16)	18.20 (9.99:25.89)	0.872[f]	15.38 (9.99:20.01)	18.70 (10.71:38.16)	18.69 (9.93:36.23)	0.156[f]	19.54 (11.58:38.16)	17.32 (9.93:36.23)	**0.003[c]**
IPM highest apex-LFR	20.20 ± 4.57	23.43 ± 4.71	**0.002[d]**	21.94 (13.06:41)	22.94 (14.69:29.92)	23.85 (10.49:32.21)	0.523[f]	18.20 (10.49:20.06)	23.96 (13.06:30.82)	23 (12.04:41)	**0.006[f]**	22.66 ± 4.57	22.75 ± 4.97	0.928[d]
Distance between bases	17.30 (5.33:29.71)	19.11 (9.17:41.07)	**0.016[c]**	17.62 ± 4.82	19.86 ± 5.60	20.54 ± 5.90	0.093[g]	22.70 (14.92:26.31)	20.01 (10.44:41.07)	18.02 (5.33:33.47)	0.264[f]	19.24 (9.17:33.47)	18.35 (5.33:41.07)	0.410[c]
Distance between apexes	24.75 ± 7.02	25.72 ± 7.13	0.539[d]	24.08 (10.70:37.37)	24.99 (12.06:43.02)	27.63 (12.07:41.28)	0.113[f]	21.25 ± 4.62	19.76 ± 5.05	18.91 ± 5.88	0.258[g]	25.63 ± 7.59	25.47 ± 6.95	0.915[d]
SPM-AAM	50.63 ± 6.45	48.19 ± 6.02	0.074[d]	49.94 ± 6.51	47.50 ± 5.84	48.68 ± 6.04	0.205[g]	45.37 (43.34:61.27)	49.13 (38.03:68)	48.79 (35.17:58.70)	0.704[f]	47.84 ± 6.13	49.02 ± 6.19	0.359[d]
IPM-AAM	49.66 (42.04:75)	49.19 (35.96:72.84)	0.302[c]	50.13 (35.96:75)	48.31 (37.20:63.60)	50.09 (40.22:72.84)	0.109[f]	53.89 (43.75:72.84)	48.59 (35.96:75)	49.71 (38.25:68.76)	0.451[f]	50.09 (38.25:60.89)	49.09 (35.96:75)	0.988[c]
SPM-coaptation line	40.89 ± 7.31	40.06 ± 5.85	0.544[d]	41.04 ± 6.58	38.87 ± 6.12	40.81 ± 5.68	0.227[g]	39.54 (37.16:54.95)	38.49 (29.47:59.37)	38.89 (28.81:55.90)	0.820[f]	40.91 (28.81:49.93)	38.59 (29.08:59.37)	0.699[c]
IPM-coaptation line	42.40 ± 7.53	41.71 ± 6.38	0.639[d]	41.72 (29.84:58.26)	39.43 (29.53:54.93)	41.55 (30.25:59.02)	0.473[f]	47.52 ± 7.79	41.55 ± 7.13	41.57 ± 6.09	0.099[g]	41.50 (29.53:52.66)	40.37 (29.84:59.02)	0.569[c]
Intermuscular angle	21.76 (12.13:44)	23.25 (11.51:45.41)	**0.050[c]**	21.77 (11.51:36.20)	22.89 (12.17:43.44)	26.29 (14.64:45.41)	**< 0.001[f]**	25.85 (18.23:42.64)	24.09 (12.13:45.41)	22.57 (11.51:44)	0.227[f]	24.29 (11.51:43.44)	22.67 (12.13:45.41)	0.907[c]

Data are expressed as median (minimum:maximum) and mean ± standard deviation in degrees for angle measurement and mm for other measurements. [c]Mann–Whitney U test; [d]the independent samples t-test; [f]Kruskal-Wallis test; [g]ANOVA test. AAM — anterior annular midpoint; BMI — body mass index; IPM — inferior papillary muscle; LFR — left fibrous ring; PM — papillary muscle; SPM — superior papillary muscle.

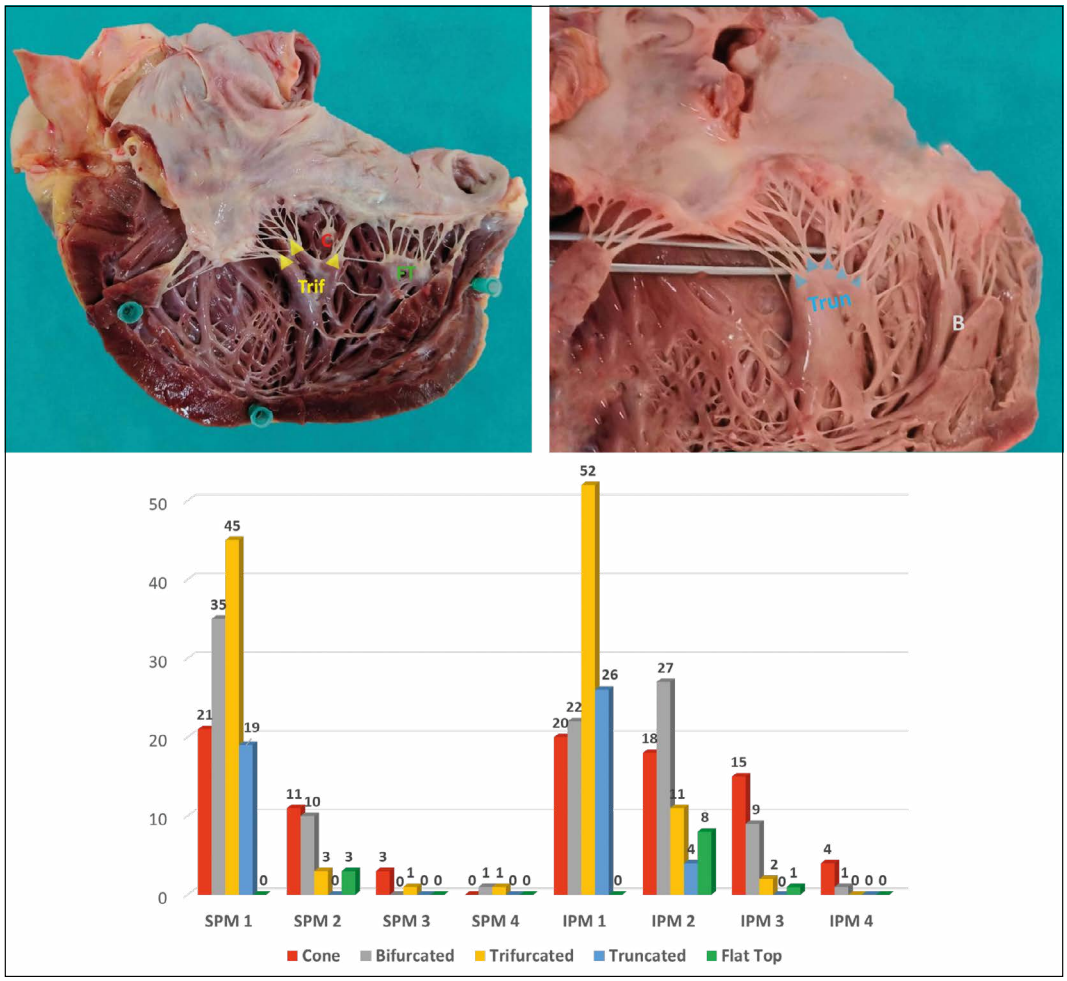

Figure 4. Shape characteristics of papillary muscles. Arrowheads — apex of papillary muscles. B — bifurcated; C — cone; FT — flat-top; IPM — inferior papillary muscle; SPM — superior papillary muscle; Trif — trifurcated; Trun — truncated.

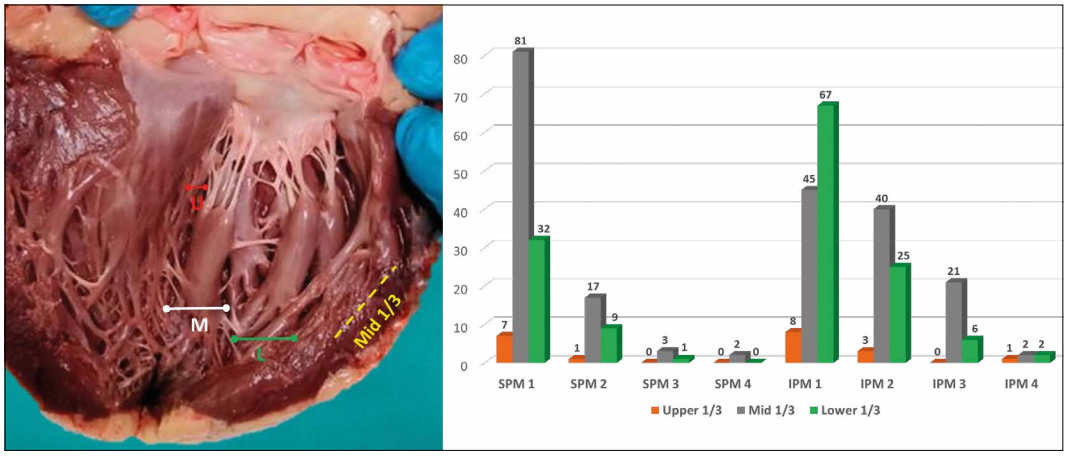

Figure 5. Origin regions of papillary muscles. IPM — inferior papillary muscle; L — lower; M — middle; SPM — superior papillary muscle; U — upper.

named anterolateral commissure (ALC) (A1–P1) and posteromedial commissure (PMC) (A3–P3) according to their locations.

The length of the leaflet tissue is critical for the leaflets to be tightly coapted and to maintain the proper position [5]. In all cases, P2 width was greater than P1 (pathological $p < 0.001$, non-pathological $p < 0.001$) and P3 (pathological $p < 0.001$, non-pathological $p < 0.001$), and P3 width was greater than P1 (pathological $p = 0.018$, non-pathological $p < 0.001$). Similarly, P2 height was found to be higher than P1 (pathological $p = 0.002$, non-pathological $p < 0.001$) and P3 (pathological $p < 0.001$, non-pathological $p < 0.001$). It was determined that the height of P1 was higher than P3 in non-pathological cases ($p = = 0.01$), and no differences were detected between the heights of the two structures in pathological cases. Additionally, PMC width and height were found to be greater than ALC ($p = 0.009$ and $p = 0.022$ in pathological cases, $p < 0.001$ and $p < 0.001$ in non-pathological cases, respectively). Although our findings were similar to those of Krawczyk et al. [12], unlike this study, there was no statistically significant difference between P3 and P1 widths. We think that this difference is due to the fact that they work with fixed hearts.

In addition, the annular widths of P1 and P3 and the height of the AML were greater in pathological cases than in non-pathological cases. Since coaptation between P1–P2–P3 is known to be as important as coaptation between AML and PML [13], leaflet tissue that prevents proper coaptation may be P1 and P3, as in the cases in this study. Accordingly, in the percutaneous end-to-end mitral valve repair technique (such as MitraClip, PASCAL) [1], a single clip placed in the A2–P2 position may be insufficient. Furthermore, the length in the AML may cause a mismatch in the A2–P2 leaflets, resulting in clip-related leaflet damage. Therefore, consideration of the information presented may help the surgeon to select the appropriate length and number of clips, increase the likelihood of success of the technique, and prevent potential complications.

Table 9. Logistic regression analysis.

			95% confidence interval	
	Odds ratio	**p-value**	**Lower bound**	**Upper bound**
Heart length	1.07	**0.049**	1.00	1.15
Heart width	1.15	**0.002**	1.05	1.26
Age	1.08	**0.002**	1.03	1.13
Body mass index	1.25	**0.004**	1.07	1.45
Model $\chi^2 = 69.49$; **p-value < 0.001**				
$R^2 = 0.633$				
Hosmer and Lemeshow test $p = 0.992$				
$n = 120$				

Tendinous cords

There is wide variability in the anatomy and branching patterns of TC. In the present study, the anatomical classification was preserved, and TC were defined in two groups as TTC and FTC. Gray's [24] reported MV-related FTCs in approximately 50% of all people, and Krawczyk et al. [11] reported that it was present in almost all cases (95%). The presence of FTC was detected in all (100%) of the 120 cases evaluated here. The number of FTC originating from SPM was 5.3 ± 2.5 and IPM was 9.2 ± 3.8, respectively. Krawczyk et al. [11] reported that an average of 3.5 ± 2.2 FTC originated from SPM and an average of 5.4 ± 2.7 from IPM. Also, as in their results, it was found that FTC originating from IPM were more numerous than SPM.

A significant number of ruptures of artificial chordae used for mitral valve repair have been reported

Table 10. Receiver Operating Characteristic (ROC) curve analysis.

	AUC	**p-value**	**Cut-off point**	**Sensitivity %**	**Selectivity %**	**PPV %**	**NPV %**
BMI	0.731	< 0.001	> 26.7	71	69.7	44.9	87.3
Heart weight [g]	0.878	< 0.001	> 414	83.9	78.7	57.8	93.3
Heart length/width ratio	0.658	0.006	≤ 1.24	87.1	41.6	34.2	90.2
MV width [mm]	0.701	< 0.001	> 99.96	64.5	69.7	42.6	84.9
LV wall thickness [mm]	0.730	< 0.001	> 15.08	41.9	97.8	86.7	82.9
Annulus ML diameter [mm]	0.696	< 0.001	> 30.71	87.1	49.9	37.5	91.7
Annular area [mm^2]	0.625	0.003	> 619.37	67.7	62.9	38.9	84.8

AUC — area under the ROC curve; BMI — body mass index; LV — left ventricle; ML — mediolateral; MV — mitral valve; NPV — negative predictive value; PPV — positive predictive value.

in the literature [25]. They concluded that increasing the number of neo-chordae and sizing them to the correct length is essential for a more durable mitral valve repair [25]. This is because TC interfere with the mitral leaflets structure, contribute to their fibrous skeleton, and, due to their complex arrangement, provide an even distribution of stress on the mitral leaflets [15]. We believe that not only disconnected TTCs but also disconnected FTCs should be considered in the planning of artificial CT to ensure proper stress distribution of neo-chordae on the leaflets. FTCs, like TTCs, also participate in leaflet stress and their number is quite high as seen in this study. However, when the studies are analyzed, we think that they are often ignored, leading incorrect leaflet stress. In addition, although the number of new cords is often the focus in the literature, we believe that the implant location of these cords (Tab. 6) is also important in creating appropriate leaflet stress.

Papillary muscles

Papillary muscles contract during ventricular systole, pulling the leaflets into the ventricles through TC, preventing the backflow of blood into the atria. Dysfunction of PMs causes the leaflets to not close properly during ventricular systole. Resulting in blood flowing back into the atrium. There are many types of surgeries, such as resection, repositioning, and realignment, to restore the normal physiological function of PMs [9]. If there is more than one PM, the number of options for deciding the direction and degree of realignment increases, facilitating the maintenance and restoration of normal physiological function [9]. Our findings regarding papillary muscle and apex numbers and sizes are consistent with the literature [9, 11]. In addition, it was reported that PMs grow in length to meet the chronically increased workload or in width to create more tension in pathological conditions [8]. This study confirms this by showing that PMs were longer in pathological hearts (SPM $p = 0.005$, IPM $p < 0.001$).

The location of the PMs in the LV is defined as its spatial configuration. The spatial location of PMs can be described mathematically, especially by considering measurements such as their distance from the mitral annulus or mitral coaptation [20]. In this context, different annulo-papillary distances were defined in many studies. Sakai et al. [22] made 4 different measurements from PM apex to annulus at 2, 4, 8, and 10 o'clock directions. Kim et al. [10] defined the distance from the ends of the PMs to the AAM as "tethering distance". Krawczyk et al. [11] evaluated the highest PM apex-LFR distance. Although different annulo-papillary distances were defined, researchers agree that annulo-papillary continuity is important for the normal functioning of the LV and proper coaptation, and this relationship must be maintained in valve replacement to reduce thus the risk of post-op complications [10, 20]. However, we think that the data may be insufficient in cases where PM reconstruction and/or repositioning is required in studies where the apex is defined as the reference point. Therefore, in this study, the distances of the midpoint of the bases of the PMs to the AAM and the coaptation line (Tab. 1), as well as the highest apex-LFR distances of the PMs were recorded (Tab. 8).

The shape of PMs affects the passage of blood through the LV [3]. It was reported that conical, broad-based, distant from the center of the ventricular cavity, and narrow apex muscles best facilitate cardiovascular physiology with minimal obstruction to blood flow [9]. For this reason, there are many studies investigating and categorizing PM shapes [3, 21]. While Bhadoria et al. [3] classified PMs as broad apex, pyramidal, fan-shaped and cone-shaped, Saha et al. [21], similar to this study (Fig. 4), determined 5 muscle shapes: cone, bifurcated, trifurcated, truncated, and flat-top. Furthermore, the location of the PMs has primary importance for normal cardiovascular physiology, as it influences the alignment of the TC and the direction of traction on the ventricular wall [9]. For this reason, the origin regions of the papillary muscles from the ventricular wall were examined and, similar to the literature [21], it was observed that both muscle groups mostly originated from the middle 1/3 part (Fig. 5).

CONCLUSIONS

The fixation process is a chemical reaction, and it must be taken into account that it may cause changes in the size and shape of the structure, which might cause differences in measurements. We believe that our data will be closer to live conditions when

compared to the studies performed on fixed hearts in the previous literature.

The present study includes the morphometric and morphological data of the LAVC components in cases with and without CVD, and also includes the comparison with the demographic characteristics of the cases. Accordingly, all parameters related to the heart and left ventricle (heart weight, heart length, heart width, MV width, left ventricular and apex wall thicknesses, LVIT–LVOT distances and diameters), ML diameter of annulus and annular area, P1 and P3 leaflet width, AML height, and papillary muscle dimensions were found to increase in cases with CVD. Heart length and width, as well as the age and BMI of the individuals, were identified as the main risk factors for the presence of CVD. BMI, heart weight, heart length/ /width ratio, MV width, LV wall thickness, annular area, and ML diameter of annulus were found to be important diagnostic criteria in the determination of CVD. In conclusion, this study provides anatomical information and recommendations for proper coaptation, preservation of left ventricular function, and correction of technical errors reported in previous studies in mitral valve repair and replacement surgeries. Therefore, we believe that our findings will help clinicians in the diagnosis, treatment plan, and management of the surgical process of pathologies involving the LAVC and will shed light on increasing the success rate of new techniques.

ARTICLE INFORMATION AND DECLARATIONS

Data availability statement

Original contributions are included in the manuscript. Further questions can be directed to the corresponding author.

Ethics statement

The study was reviewed and approved by an Ethics Committee.

Author contributions

BN Çandır: project development, data collection, data analysis, manuscript writing/ editing. C Ergin: project development, data collection. K Yılar: data collection, project development. O Coşkun: project development, data collection. E Kara: data collection, data management. A Kale: manuscript editing, data analysis. N Bozbuğa: project development, manuscript editing. A Öztürk: project development, manuscript editing. O Gayretli: project development, data collection, manuscript writing/editing.

Funding

None.

Conflict of interest

The authors declare that they have no conflict of interest.

REFERENCES

1. Al-Azizi K, Szerlip M. Mitral stenosis after mitraclip: how to avoid and how to treat. Curr Cardiol Rep. 2020; 22(7): 50, doi: 10.1007/s11886-020-01301-5, indexed in Pubmed: 32500412.
2. Baxi AJ, Restrepo CS, Vargas D, et al. Hypertrophic cardiomyopathy from A to Z: genetics, pathophysiology, imaging, and management. Radiographics. 2016; 36(2): 335–354, doi: 10.1148/rg.2016150137, indexed in Pubmed: 26963450.
3. Bhadoria P, Bisht K, Singh B, et al. Cadaveric study on the morphology and morphometry of heart papillary muscles. Cureus. 2022; 14(2): e22722, doi: 10.7759/cureus.22722, indexed in Pubmed: 35382408.
4. Carpentier A, Branchini B, Cour JC, et al. Congenital malformations of the mitral valve in children. J Thorac Cardiovasc Surg. 1976; 72(6): 854–866, doi: 10.1016/s0022-5223(19)40003-2, indexed in Pubmed: 994536.
5. Dal-Bianco JP, Levine RA. Anatomy of the mitral valve apparatus: role of 2D and 3D echocardiography. Cardiol Clin. 2013; 31(2): 151–164, doi: 10.1016/j.ccl.2013.03.001, indexed in Pubmed: 23743068.
6. Faletra FF, Leo LA, Paiocchi VL, et al. Anatomy of mitral annulus insights from non-invasive imaging techniques. Eur Heart J Cardiovasc Imaging. 2019; 20(8): 843–857, doi: 10.1093/ehjci/jez153, indexed in Pubmed: 31219549.
7. Flachskampf FA, Chandra S, Gaddipatti A, et al. Analysis of shape and motion of the mitral annulus in subjects with and without cardiomyopathy by echocardiographic 3-dimensional reconstruction. J Am Soc Echocardiogr. 2000; 13(4): 277–287, doi: 10.1067/mje.2000.103878, indexed in Pubmed: 10756245.
8. Freedman JE. Circulation research. Circ Res. 2019; 125(1): 5–6, doi: 10.1161/circresaha.119.315412.
9. Gunnal SA, Wabale RN, Farooqui MS, et al. Morphological variations of papillary muscles in the mitral valve complex in human cadaveric hearts. Singapore Med J. 2013; 54(1): 44–48, doi: 10.11622/smedj.2013011, indexed in Pubmed: 23338917.
10. Kim K, Kaji S, An Y, et al. Interpapillary muscle distance independently affects severity of functional mitral regurgitation in patients with systolic left ventricular dysfunction. J Thorac Cardiovasc Surg. 2014; 148(2): 434–440.e1, doi: 10.1016/j.jtcvs.2013.09.029, indexed in Pubmed: 24189316.

11. Krawczyk-Ożóg A, Hołda MK, Bolechała F, et al. Anatomy of the mitral subvalvular apparatus. J Thorac Cardiovasc Surg. 2018; 155(5): 2002–2010, doi: 10.1016/j.jtcvs.2017.12.061, indexed in Pubmed: 29397976.
12. Krawczyk-Ożóg A, Hołda MK, Sorysz D, et al. Morphologic variability of the mitral valve leaflets. J Thorac Cardiovasc Surg. 2017; 154(6): 1927–1935, doi: 10.1016/j.jtcvs.2017.07.067, indexed in Pubmed: 28893395.
13. Lai DT, Tibayan FA, Myrmel T, et al. Mechanistic insights into posterior mitral leaflet inter-scallop malcoaptation during acute ischemic mitral regurgitation. Circulation. 2002; 106(12 Suppl 1): I40–I45, indexed in Pubmed: 12354707.
14. Lee PT, Dweck MR, Prasher S, et al. Left ventricular wall thickness and the presence of asymmetric hypertrophy in healthy young army recruits: data from the LARGE heart study. Circ Cardiovasc Imaging. 2013; 6(2): 262–267, doi: 10.1161/CIRCIMAGING.112.979294, indexed in Pubmed: 23307776.
15. McCarthy KP, Ring L, Rana BS. Anatomy of the mitral valve: understanding the mitral valve complex in mitral regurgitation. Eur J Echocardiogr. 2010; 11(10): i3–i9, doi: 10.1093/ejechocard/jeq153, indexed in Pubmed: 21078837.
16. Messika-Zeitoun D, Nickenig G, Latib A, et al. Transcatheter mitral valve repair for functional mitral regurgitation using the Cardioband system: 1 year outcomes. Eur Heart J. 2019; 40(5): 466–472, doi: 10.1093/eurheartj/ehy424, indexed in Pubmed: 30124798.
17. Mohammadi S, Hedjazi A, Sajjadian M, et al. Study of the normal heart size in Northwest part of Iranian population: a cadaveric study. J Cardiovasc Thorac Res. 2016; 8(3): 119–125, doi: 10.15171/jcvtr.2016.25, indexed in Pubmed: 27777697.
18. Mrsic Z, Hopkins SP, Antevil JL, et al. Valvular heart disease. Prim Care. 2018; 45(1): 81–94, doi: 10.1016/j.pop.2017.10.002, indexed in Pubmed: 29406946.
19. Muresian H. The clinical anatomy of the mitral valve. Clin Anat. 2009; 22(1): 85–98, doi: 10.1002/ca.20692, indexed in Pubmed: 18773480.
20. Oliveira D, Srinivasan J, Espino D, et al. Geometric description for the anatomy of the mitral valve: a review. J Anat. 2020; 237(2): 209–224, doi: 10.1111/joa.13196, indexed in Pubmed: 32242929.
21. Saha A, Roy S. Papillary muscles of left ventricle-morphological variations and it's clinical relevance. Indian Heart J. 2018; 70(6): 894–900, doi: 10.1016/j.ihj.2017.12.003, indexed in Pubmed: 30580862.
22. Sakai T, Okita Y, Ueda Y, et al. Distance between mitral anulus and papillary muscles: anatomic study in normal human hearts. J Thorac Cardiovasc Surg. 1999; 118(4): 636–641, doi: 10.1016/S0022-5223(99)70008-5, indexed in Pubmed: 10504627.
23. She JQ, Guo JJ, Yu YF, et al. Left ventricular outflow tract obstruction in hypertrophic cardiomyopathy: the utility of myocardial strain based on cardiac MR tissue tracking. J Magn Reson Imaging. 2021; 53(1): 51–60, doi: 10.1002/jmri.27307, indexed in Pubmed: 32798304.
24. Standring S. Gray's anatomy: the anatomical basis of clinical practice. 39th ed. Elsevier Churchill Livingstone, London 2005.
25. Vendramin I, Milano AD, Pucci A, et al. Artificial chordae for mitral valve repair. J Card Surg. 2022; 37(11): 3722–3728, doi: 10.1111/jocs.16937, indexed in Pubmed: 36116053.
26. Walmsley R. Anatomy of left ventricular outflow tract. Br Heart J. 1979; 41(3): 263–267, doi: 10.1136/hrt.41.3.263, indexed in Pubmed: 426974.
27. Yamamoto K, Mori S, Fukuzawa K, et al. Revisiting the prevalence and diversity of localized thinning of the left ventricular apex. J Cardiovasc Electrophysiol. 2020; 31(4): 915–920, doi: 10.1111/jce.14386, indexed in Pubmed: 32090387.